PAPER

Check for updates

Reactivity and stability synergism directed by the electron transfer between polyoxometalates and metal–organic frameworks†

Xinlin Lu, Ting Cheng, Yurii V. Geletii, [iD] * John Bacsa and Craig L. Hill [iD] *

The synergism between polyoxometalates (POM) and Cu(II) ions in homogeneous aerobic thiol oxidative deodorization has been realized in a more utilitarian heterogeneous catalyst: a multi-electron-capable POM captured in the pores of a metal–organic framework (MOF), HKUST-1 (POM@HKUST). The synergism between POM and the Cu(II) nodes in the MOF depends on the type of POM. Phosphovanadomolybdates, $PV_xMo_{12-x}O_{40}^{(3+x)-}$ (x = 1–3) (**PVMo**) but not transition-metal-substituted polytungstates PXW_{11} (X = V, Co, Zn and Co) result in POM@MOF materials that exhibit synergy relative to the individual structural components, the POM or MOF alone, not only for reactivity as in the case for the analogous homogeneous catalysts, but also for catalyst structural stability. The **PVMo**@HKUST-catalyzed reaction proceeds to essentially 100% conversion and the material is recoverable and unchanged based on FTIR spectroscopy, powder XRD data and other observations after reaction. The **PXW$_{11}$**@HKUST materials produce only limited conversions and decompose to white powders after reaction. X-ray photoelectron spectroscopy reveals that all the Cu(II) sites in the HKUST-1 become Cu(I) sites that are stable in air. Further kinetics studies show that **PVMo** undergoes fast multielectron transfer with intermediate Cu/RSH complexes, while **PXW$_{11}$** show far slower and limited electron transfer ability with these Cu/RSH complexes. Limited electron transfer between Cu nodes and the encapsulated POM units not only hinders reactivity but also leads to MOF framework distortion and subsequent decomposition induced by the reduction of Cu(II) to Cu(I) sites in the framework.

Introduction

POM@MOF composites comprising polyoxometalates (POMs) residing in metal–organic framework (MOF) pores[1–4] have been reported as catalysts for oxidative, electrocatalytic, photocatalytic and other reactions.[3–6] A central point of interest is that they can combine the attractive properties of POMs and also those of MOFs. POMs have been investigated as catalysts for years,[7–10] resulting from one or more of their following attributes: strong acidity,[11,12] facile redox chemistry,[13–16] photoactivity[17–22] and multielectron transfer ability.[17,23,24] POMs in conventional solid phases, not pseudo-liquid phases,[25] have small surface areas but are soluble in aqueous and many organic solvents. Thus, the immobilization of POMs on porous materials, including polymers,[26] covalent organic frameworks (COFs),[27] zeolites[28] and MOFs,[29–32] is attractive because it converts these homogeneous catalysts into more utilitarian heterogeneous ones with substantial surface area.

Among all POM supports, MOFs, such as MIL-101,[33–35] MOF-199 (HKUST-1),[4,36–38] NU-1000,[39–42] UIO-66 (ref. 43–46) and ZIF-8 (ref. 47–49) are highly attractive host materials because they offer high porosity and sufficient pore (cage) size to encapsulate POMs, including Keggin,[37] Wells–Dawson[43] and sandwich structural families,[50] as guest materials forming POM@MOF composites.

Recent work in our group[51,52] reveals strong synergism effect between Cu(II) ion and phosphovanadomolybdates, $PV_xMo_{12-x}O_{40}^{(3+x)-}$ (x = 1–6) (**PVMo**) for catalysis of air-based oxidative removal of odorous thiols, facilitated by the redox buffering effect of **PVMo**. Moreover, the redox buffering and synergism are only operative for **PVMo** and not phosphovanadotungstates, $PV_xW_{12-x}O_{40}^{(3+x)-}$ (x = 1, 3, 6) (**PVW**). Triggered by this, we sought formulation of a solid and thus more useful catalyst for aerobic thiol deodorization by combining Cu(II) and POM together as a heterogeneous catalyst. Here, we use the POM, HKUST-1 with Cu-containing nodes to bring Cu(II) and reversible multi-electron POM centers into proximity (POM@HKUST, Fig. 1). HKUST-1, in addition to providing well-ligated Cu(II), contains large pores that accommodate Keggin POMs with their accompanying counter-cations in the smaller pores. Various Keggin POMs have been incorporated into HKUST-1 for oxidation,[36,53–59]

Department of Chemistry, Emory University, Atlanta, GA 30322, USA.
E-mail: iguelet@emory.edu, chill@emory.edu

† Electronic supplementary information (ESI) available. CCDC 2256821. For ESI and crystallographic data in CIF or other electronic format see DOI: https://doi.org/10.1039/d3cy00569k
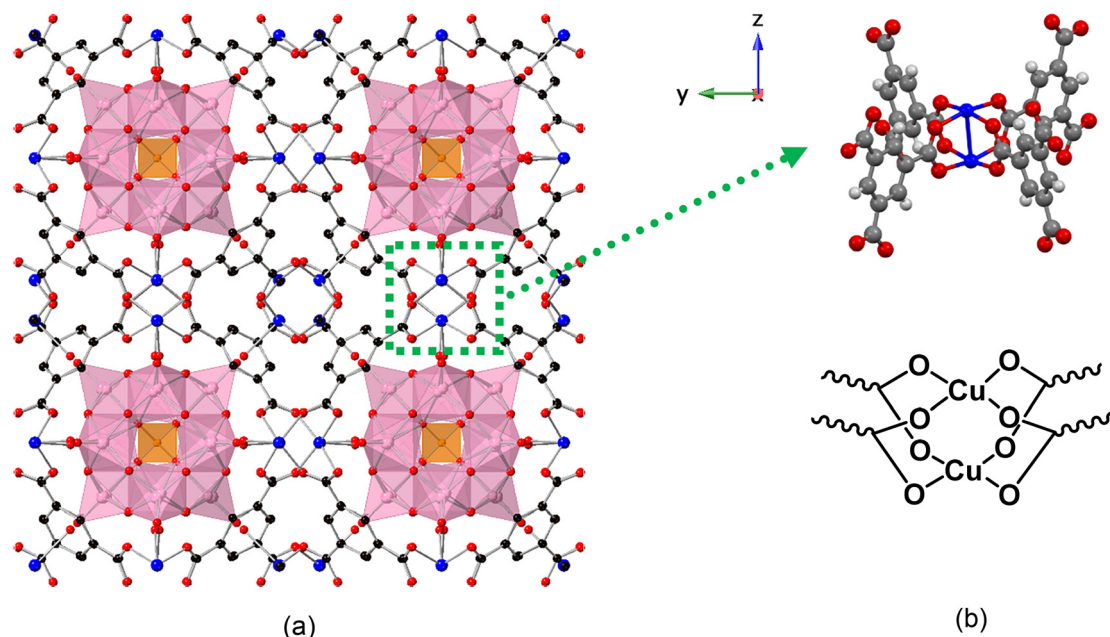
Fig. 1 (a) X-ray single-crystal structure of **PV$_2$Mo$_{10}$**@HKUST [100] direction. The purple polyhedral represent the MoO$_6$ (or VO$_6$) and orange tetrahedra represent the PO$_4$ units in the POM. The HKUST-1 framework is represented in ball-and-stick form. C is black, O is red, Cu is blue. The tetramethylammonium (TMA) cations reside in the smaller pores and resolve as an average of 5 per POM unit (omitted for clarity). (b) The ball and stick and chemical formula of di-copper node.

esterification,[60,61] hydrolysis[37] and other organocatalytic reactions.[62] Many efforts have been made to increase the catalytic activity such as tuning the nanocrystal size,[53] modifying the morphology,[60] designing the hierarchical structure[57] and regulating the pore size.[63] Incorporating Keggin POMs into HKUST-1 not only increases the thermal[64] and hydrolytic[36] stability of the MOF but also increases the reactivity of the POM with a marked synergy between POM and MOF framework.[36,53–55] However, almost all the synergism reported previously is due to the MOF framework confinement effect that enhances the absorption, selectivity, and conversion of organic substrates, while POM is the real catalytic center of the reaction.[53–55] In this work, we show that the aerobic thiol oxidation mechanism involves both the Cu(II) nodes in the MOF framework and multi-electron redox processes of the POM polyanion. In addition, we show that synergistic electron transfer between MOF and POM maintains the overall POM@MOF framework.

Results and discussion

POM@MOF materials and characterization

PV$_x$Mo$_{12-x}$O$_{40}$$^{(3+x)-}$ (x = 0–3) (**PVMo**) were incorporated into the HKUST-1 using the well-established hydrothermal synthetic method;[37,38] however, the synthesis of POM@HKUST with **PVMo** with x > 3 using the same synthetic method failed. This likely reflects the decreasing hydrolytic stability of **PVMo** as the number of vanadium centers in the polyanion increases. We note that there are other synthetic methods to synthesize POM@HKUST materials.[53,61,65,66] This paper does not explore various

synthetic methods but only focuses on the hydrothermal approach. Thus, in this work, **PVMo**@HKUST (x = 0–3, **PVMo$_{11}$**@HKUST, **PV$_2$Mo$_{10}$**@HKUST and **PV$_3$Mo$_9$**@HKUST) are discussed. The phase purity of **PVMo**@HKUST were established by FT-IR spectra and powder X-ray diffraction (PXRD) patterns (Fig. 2a and b and S1 and S2†). The PXRD patterns were compared with the calculated patterns from the single crystal X-ray diffraction of **PV$_2$Mo$_{10}$**@HKUST (Fig. 1, S3 and Table S1†). In Keggin crystal structures, the PO$_4$ tetrahedron is disordered due to crystal symmetry, resulting in 8 positions for the mixed arrangement of the 4 O atoms. However, our study showed that if the crystals were treated as being chiral, F23, the PV$_2$Mo$_{10}$ anion resolves into a more ordered form with the tetrahedral arrangement resolved into a single component. This resolved PV$_2$Mo$_{10}$ anion was found to be packed into the pores of HKUST-1, with the terminal oxygen pointing towards the di-copper nodes. Furthermore, the crystals were found to be racemically twinned, resolving the Keggin structure. Each twin domain contained only one enantiomer, but due to the 50% twinning, the crystal had equal proportions of domains with each enantiomer. We determined that **PV$_3$Mo$_9$**@HKUST is also chiral and isostructural with **PV$_2$Mo$_{10}$**@HKUST (see ESI† for more details.) For the **PVW**, only x = 0, 1 can be inserted into HKUST-1 (**PW$_{12}$**@HKUST and **PVW$_{11}$**@HKUST). This likely derives from the fact that unlike the corresponding Mo-based Keggin POMs, the Keggin polytungstates are more rigid and far less hydrolytically labile. In addition, we succeeded in incorporating a series of transition-metal-substituted polytungstates (**PXW$_{11}$**, X = Cu, Co and Ni) into
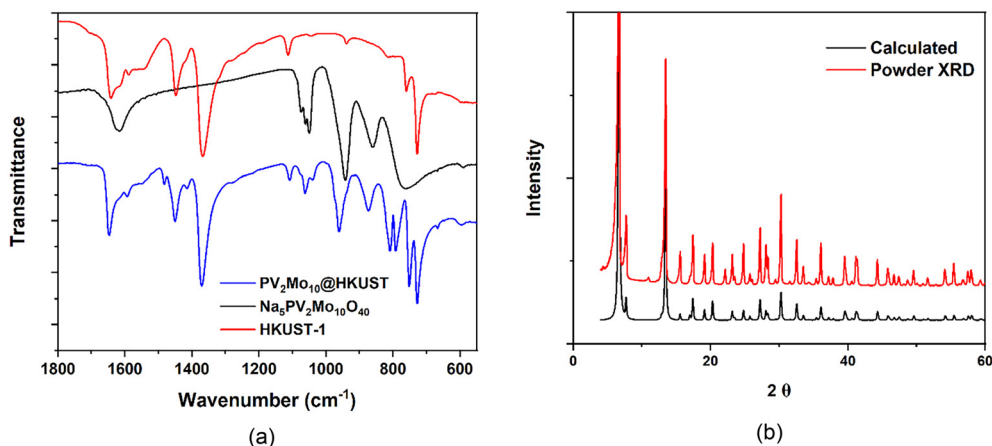
This journal is © The Royal Society of Chemistry 2023

Catal. Sci. Technol., 2023, **13**, 5094–5103 | **5095**

Fig. 2 (a) FT-IR of $Na_5PV_2Mo_{10}O_{40}$, HKUST-1 and **PV_2Mo_{10}**@HKUST; (b) **PV_2Mo_{10}**@HKUST calculated XRD pattern from single-crystal refinement data compare with the experimental powder XRD pattern.

HKUST-1 (**PXW**@HKUST: **PCuW₁₁**@HKUST, **PCoW₁₁**@HKUST and **PNiW₁₁**@HKUST). The PXRD patterns of **PVW₁₁**@HKUST, **PCoW₁₁**@HKUST and **PNiW₁₁**@HKUST were compared with the calculated pattern from the single crystal data of **PCuW₁₁**@HKUST from previous work (Fig. S5†).[36] Interestingly, **PCuW₁₁**@HKUST and **PVW₁₁**@HKUST single crystals do not show the ordered packed POM and chiral space groups. FT-IR and PXRD and establish the phase purity of these materials Fig. S4 and S5.† The incorporated transition metal, M, in the POM was established using SEM-EDX (Fig. S6–S8†). The SEM images show that POM@HKUST materials are large bulk crystals. EDX shows clearly that the POM elements, O, P, and W, including the transition metals, V, Co and Ni, are present in these crystalline materials. Nitrogen isotherms of **PV₂Mo₁₀**@HKUST and **PCoW₁₁**@HKUST (Fig. S24†) show the specific surface areas are 619.2 and 413.5 $m^2\ g^{-1}$, respectively. Comparing with the HKUST-1 alone, 1264 $m^2\ g^{-1}$,[36] the smaller specific surface area can attribute to the successful insertion of the POMs.

POM leaching and solvent selection

The leaching of POM from MOF pores during the reaction is a potential issue for POM@MOF materials.[3,4] Fig. 3a shows the thiol (RSH) oxidation reactivity of **PV₂Mo₁₀**@HKUST in different organic solvents (see thiol oxidation section in ESI†). Auto-catalytic behavior is seen in acetonitrile (AN) and dimethylacetamide (DMA). This is because POM is leached into the solution during reaction in these polar POM-solubilizing solvents, and the dominant mode of catalysis switches from heterogeneous to homogeneous by POM in solution. To further address POM leaching from MOF pores in these catalytic studies, we developed a colorimetric method to detect whether POM is extracted into the solution. Supernatants were filtered after the oxidation reaction, then $SnCl_2$, a strong reducing agent, was added to the Ar-purged, filtered solution. Since $Mo(VI)$–$Mo(V)$ intervalence charge transfer band has very high extinction coefficient around 600–800 nm,[67] even a trace amount of POM that leaks into the solution is rapidly reduced and quantified by UV-vis
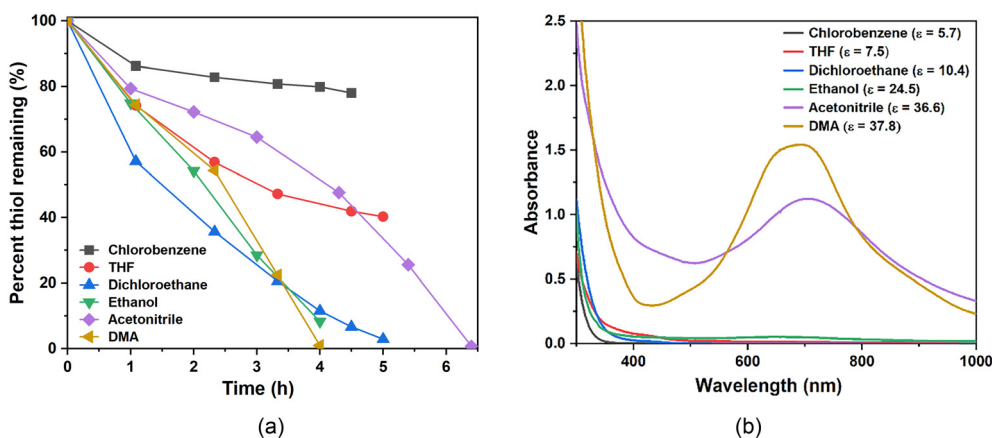

Fig. 3 (a) RSH consumption catalyzed by **PV₂Mo₁₀**@HKUST in different solvents. Conditions: dichloroethane (5 mL), 2-mercaptoethanol (28.6 mM), catalyst (0.774 mM), reaction at 50 °C. (b) UV-vis absorbance of the reduced supernatant solution after addition of $SnCl_2$ under argon after reaction.

5096 | *Catal. Sci. Technol.*, 2023, **13**, 5094–5103

This journal is © The Royal Society of Chemistry 2023

spectroscopy. Fig. 3b shows the UV-vis results. When ethanol is used as a solvent, a slight absorbance due to reduced POM in solution is observed; when AN and DMA are used, large absorbances are observed. When solvents less polar than ethanol are used, no absorbances around 600–800 nm are generated. Here we use dielectric constant (ε) to differentiate and quantify the polarity of the organic solvents. The reactivity increases as ε increases (Fig. 3b), however, when ε is too large (ethanol, 24.6), the POM starts to leach from the MOF pores. As a consequence, we chose dichloroethane for all the catalytic studies.

Activity and stability synergism

A core thrust of this study is to determine whether the synergism between **PVMo** and Cu(II) in homogeneous solution can still exist while both parts are confined without free diffusion. The aerobic oxidation of RSH catalyzed homogeneously by **PVMo** and Cu(II) in dichloroethane (30% acetonitrile for POM solubility) was evaluated (Fig. 4c and d). The same results were obtained in pure acetonitrile,[51,52] *i.e.* catalytic activity increases with increasing number of V centers

in the POM. Notably, neither Cu(II) ion nor POM alone (**PVMo**, x = 1–3, but not x = 0) have significant activity which proves a synergy exists between these two catalytic components. The conversion and turnover frequency (TOF) data for all POM@HKUST catalyzing aerobic RSH oxidation are summarized in Table S2.† The consumption curves of **PVMo**@HKUST (x = 0–3) are shown in Fig. 4a. The catalytic activity, as for the homogeneous **PVMo**/Cu catalytic systems, increases with increasing number of vanadium centers in **PVMo**. Nearly 100% conversion is achieved in 3 h, 6 h and 15 h by **PV₃Mo₉**@HKUST, **PV₂Mo₁₀**@HKUST and **PVMo₁₁**@HKUST, respectively. **PMo₁₂**@HKUST does not achieve 100% after 24 h and HKUST-1 alone converts only 45% after 20 h (Fig. 4b). **PXW**@HKUST (X = V, Cu, Co and Ni) have much lower catalytic activity than **PVMo**@HKUST, Fig. 4b. The biphasic thiol consumption kinetics in the polytungstate@HKUST systems reflects initial rapid uptake of the thiol into the POM@MOF pores, followed continued but slower thiol uptake that parallels the time-dependent decomposition of the polytungstate@HKUST systems (see discussion below). Changing the transition metal in the POM does not have a significant effect on activity. **PXW**@HKUST do not achieve
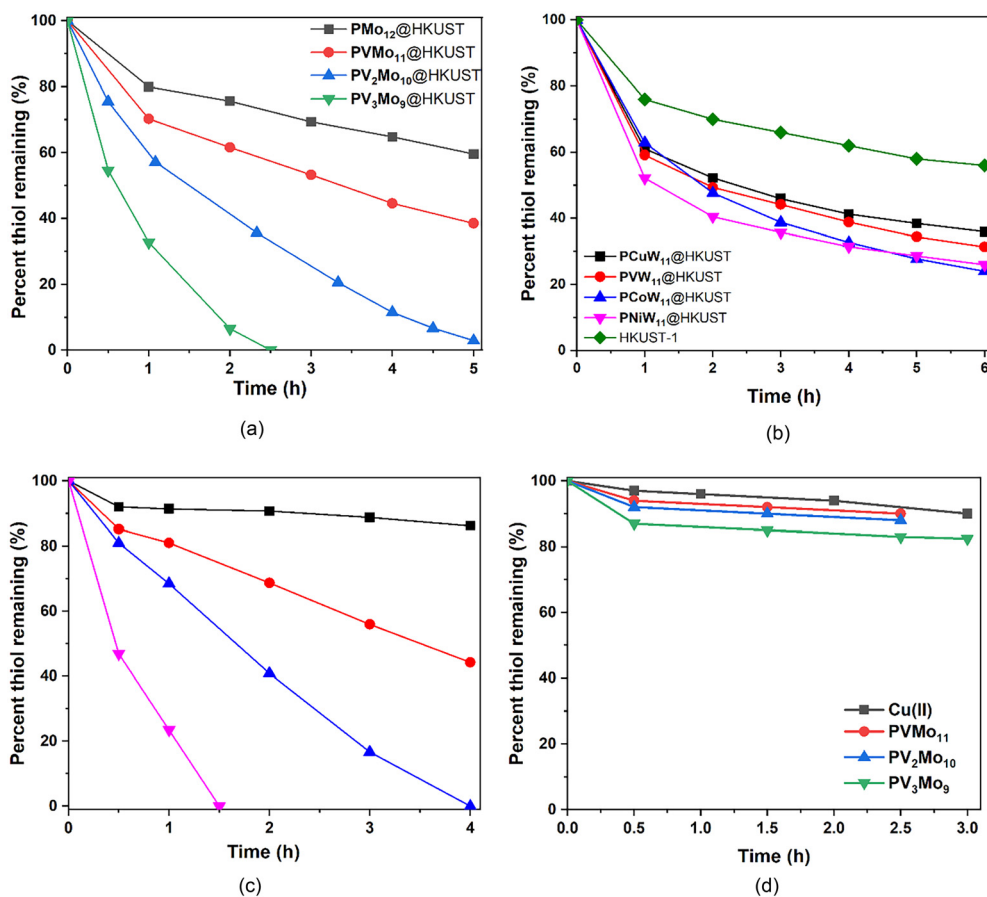
Fig. 4 RSH (28.6 mM) consumption catalyzed by (a) **PVMo**@HKUST (n = 0–3) (20 mg); (b) HKUST-1 alone (20 mg) and by **PXW**@HKUST (X = Cu, V, Ni and Co) (23 mg) in dichloroethane (5 mL) at 50 °C under air. (c) Aerobic RSH (30 mM) oxidation catalyzed by POM (0.2 mM) with Cu(II) (1.0 mM) at room temperature in a dichloroethane/acetonitrile 30% (v/v) solvent system. Black: $H_3PMo_{12}O_{40}$ (**PMo₁₂**); red: $H_4PVMo_{11}O_{40}$ (**PVMo₁₁**); blue: H_5-$PV_2Mo_{10}O_{40}$ (**PV₂Mo₁₀**); pink: $H_6PV_3Mo_9O_{40}$ (**PV₃Mo₉**). (d) Aerobic RSH (30 mM) oxidation activity in the presence of Cu(II) (0.5 mM) alone or POM (0.5 mM) alone.

100% conversion after 24 h. A homogeneous aerobic catalytic RSH oxidation investigation reveals no synergistic effect between the phosphotungstate POMs and Cu(II) ion (Fig. S9†). The same Keggin POMs were incorporated into the Cu-free large-pore MIL-101 MOFs (Fig. S10†). POM@MIL-101 materials have been widely studied.[33,34,68–71] The hydrothermal synthesis described in literature has been used in this work (see ESI† for synthesis detail).[72] Fig. S11† gives the FT-IR of all POM@MIL-101 materials that are consistent with the insertion of POMs into the MIL-101 pores.[68,73] The resulting POM@MIL-101 binary materials have very little activity implicating a direct role of the HKUST-1 Cu(II) centers in catalytic aerobic thiol oxidation.

Interestingly, the Cu–POM synergy is not limited to catalytic activity: it also extends to catalyst stability. **PVMo@HKUST** are stable during the oxidation reactions (Fig. S12† compares spectra before and after 37 equivalents of thiol are converted). Fig. 5a and b show that both the FT-IR spectra and PXRD patterns of **PV₃Mo₉@HKUST** are the same before and after reaction consistent with structural integrity of both the POM and MOF components. In contrast, the FT-IR of HKUST-1 shows that this MOF is destroyed after oxidation (Fig. 5c). Thus, there is a dramatic oxidative stabilization of the MOF framework when these Keggin POMs are incorporated into the MOF pores. Significantly, all the **PXW@HKUST** materials decompose to white powders after

reaction (Fig. S13 and S14†). Fig. 5d shows the FT-IR of **PVW₁₁@HKUST**. The C=O stretches (1644 cm⁻¹) and C–O stretches (1368 cm⁻¹) shift indicating changes in the MOF structures. This POM stabilization of the POM@MOF framework during the oxidation reaction, is POM selective: only phosphomolybdates but not phosphotungstates facilitate MOF stabilization. These data collectively indicate that the reactivity synergism between Cu(II), the MOF framework and the POM is crucial for stability of these hybrid materials.

We turn to X-ray photoelectron spectroscopy (XPS) to further probe decomposition of the **PXW@HKUST** materials. The spectra of POM@HKUST before and after reaction were collected. Fig. 6a shows the Cu 2p spectra of **PV₃Mo₉@HKUST**. Peaks at 935.1 eV and 955.1 eV belong to Cu^{2+} $2p_{3/2}$ and $2p_{1/2}$, and are accompanied by satellite peaks at 944.5 and 940.5 eV.[74–76] There are no detectable peaks due to Cu^{1+} indicating all Cu has been reoxidized back to its initial oxidation state after reaction. **PCuW₁₁@HKUST** before reaction shows Cu^{2+} 2p peaks, and Cu^{1+} $2p_{3/2}$ and $2p_{1/2}$ peaks at 933.0 and 952.9 eV, respectively. This is consistent with charge transfer between Cu^{2+} nodes and POM.[75–80] Here, we found that under the hydrothermal synthesis conditions, the transition-metal-substituted phosphotungstates prefer to undergo electron transfer with HKUST-1 (Fig. S16†) than

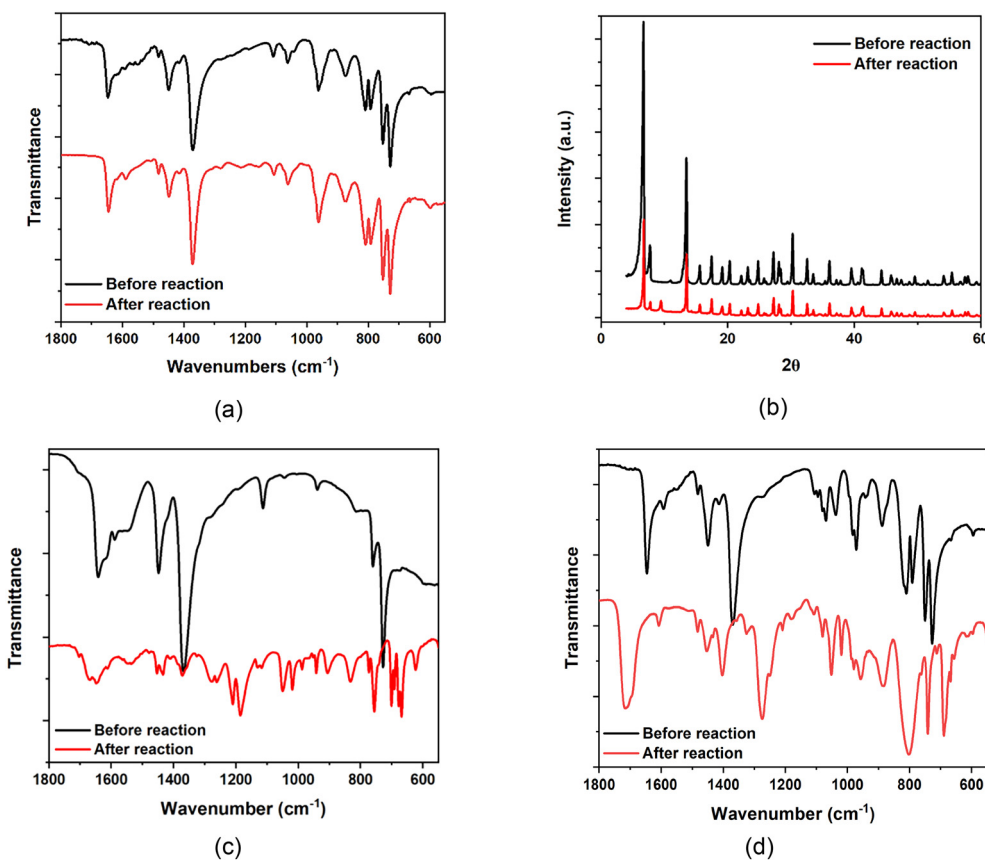**Fig. 5** (a) FT-IR and (b) PXRD spectra of **PV₃Mo₉@HKUST** before and after reaction. FT-IR spectra of (c) HKUST-1 and (d) **PVW₁₁@HKUST** before and after reaction.
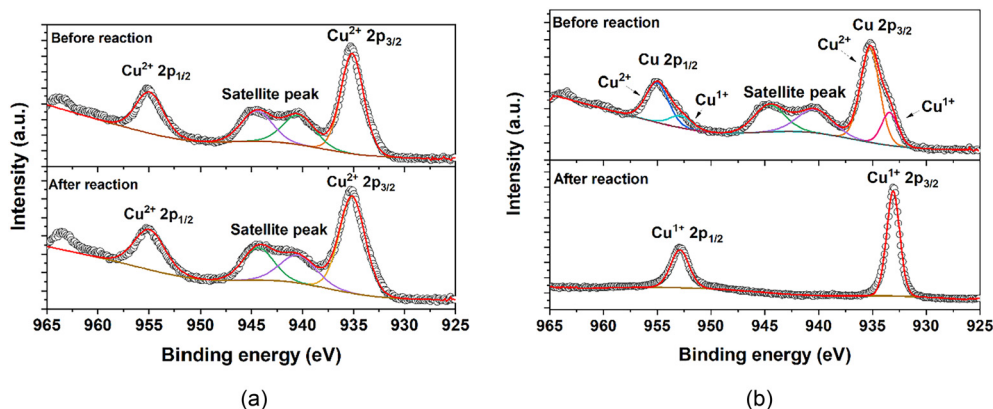
5098 | *Catal. Sci. Technol.*, 2023, **13**, 5094–5103

This journal is © The Royal Society of Chemistry 2023

Fig. 6 Cu 2p XPS spectra of POM@MOF before and after reaction: (a) **PV₃Mo₉@HKUST**; (b) **PCuW₁₁@HKUST**.

PVMo (Fig. S15†). Since even perfect HKUST-1 crystals have Cu^{1+} defects,[79] all the POM@MOF materials may contain low percents of Cu^{1+} in their nodes. Moreover, Fig. 6b shows that after reaction, the Cu^{2+} 2p peak and corresponding satellite peaks disappear, and only Cu^{1+} 2p peaks are evident. This indicates that the HKUST-1 framework breaks down and generates a Cu^{1+}-based structure that is stable when exposed to ambient air. This also directly implicates a redox role for the Cu centers in the MOF nodes. Its structural distortion results from a lack of reoxidation of Cu^{1+} to Cu^{2+}.

The mechanism of RSH oxidation catalyzed by the homogeneous **PVMo**/Cu system was recently reported.[51] The heterogeneous POM@MOF requires a modified mechanism relative to freely-diffusing copper and
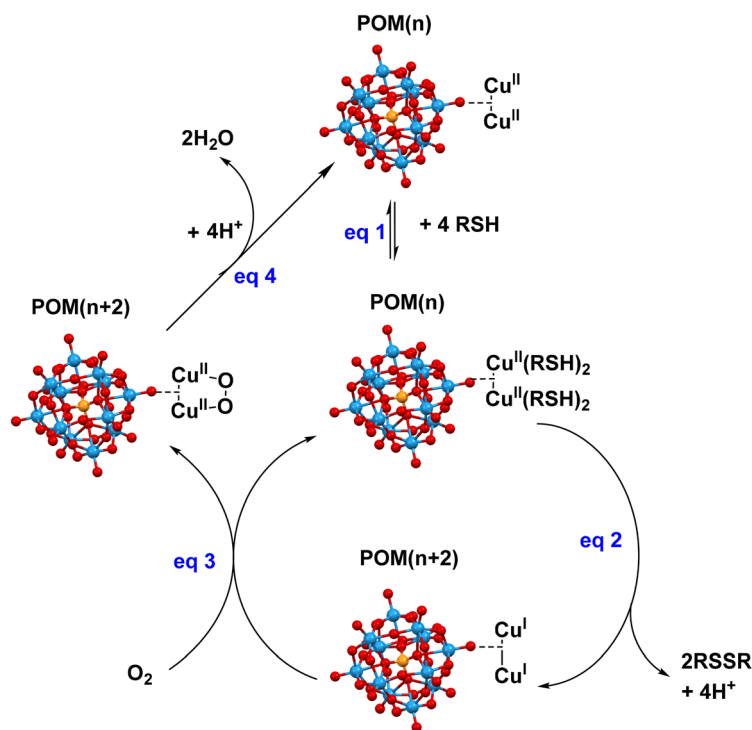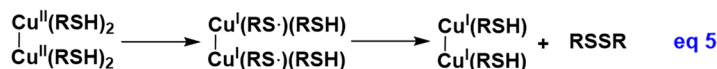

Fig. 7 Proposed mechanism of POM@MOF–catalyzed RSH aerobic oxidation.

phosphovanadomolybdate due to the confinement of Cu(II) and POM in their respective locations. The crystal structure of POM@MOF is given in Fig. 1 and S3.† Each POM is in proximity, on average, of two di-copper(II) groups. Cu, on average, binds two RSH and forms a polymeric network,[81,82] eqn (1). The $Cu^{II}(RSH)_2$ complex is a strong reducing agent, and when POM is present, the former reduces the latter by one electron to form $Cu^I(RS^{·})_2$ which then decomposes to Cu^I and RSSR products.[51] In the POM@MOF, each di-copper(II) site reduces the proximal POM by two electrons and generates a di-copper(I) site (Fig. 7, eqn (2)). One possibility for the reoxidation process is that the di-copper(I) reacts with O_2 forming a peroxo-Cu^{II} intermediate, then the peroxo group is reduced to water after receiving two electrons from a reduced POM (eqn (3) and (4))[83] However, for the PVW_{11} and PXW_{11}@HKUST materials, the decomposition to stable Cu^I sites indicates a lack of electron transfer between the POM and Cu nodes. Cu alone can catalyze the RSH oxidation in alkaline aqueous conditions,[84–88] and the mechanism is given in eqn (5). Without a POM catalyst, the di-copper sites may result in Cu^I/RSH complexes.[81,82] The XPS data suggest that the Cu^I/RSH complex is inert to O_2. The XPS survey spectra of $PCuW_{11}$@HKUST after RSH oxidation shown in Fig. S17,† compared to PV_3Mo_9@HKUST after reaction, clearly indicates a S 2p peak at 163.5 eV. For $PCuW_{11}$@HKUST, the calculated atomic content (%) of Cu and S is 6.29 and 7.35 respectively. This ratio is close to 1 : 1, and the slightly larger amount of S could be due to the trapped unreacted RSH and/or product RSSR in the MOF pores. The XPS results are consistent with the stable Cu^I site being a di-Cu^IRSH complex.

Homogeneous electron transfer between POM and the Cu/RSH complex can be studied by stopped-flow spectroscopy. Previous work[52] in aqueous buffer and acetonitrile shows that $PVMo$ (x = 1–6) can transfer multiple electrons involving both V and Mo atoms, depending on reaction conditions, while PVW (x = 1, 3 and 6) can only transfer one electron

independent of reactant concentrations. Fig. 8 shows the stopped-flow kinetics of $PVMo_{11}$ and PVW_{11} reduction in pH = 2 H_2SO_4/Na_2SO_4 buffer and $PCoW_{11}$ and $PNiW_{11}$ reduction in pH = 5 sodium acetate buffer by RSH catalyzed by μM quantities of Cu(II) under Ar (the pH changes according to the stability of POM). $PVMo_{11}$ exhibits two-stage kinetics that involves the Mo redox couple, while PVW_{11} only accepts one electron on a V atom; the W centers are not involved. The Cu concentration dependence is given in Fig. S18.† $PVMo_{11}$ is reduced by more than two electrons with increasing the Cu concentration, while PVW_{11} is only reduced by one electron independent of Cu concentration. The transition-metal-substituted polytungstates are not reduced by the Cu/RSH complex (Fig. 8). Calibration of the extinction coefficient based on the number of electrons was done by UV-vis spectra in conjunction with bulk electrolysis, Fig. S19.† Based on our proposed mechanism above, the POM should have multielectron transfer ability with di-copper thiol complexes. Therefore, the synergistic effects of the $PVMo$@HKUST materials derive from fast, multi-electron transfer between POM and the Cu nodes in the MOF.

Cyclic voltammograms (CVs) show that $PVMo_{11}$ and PVW_{11} have similar V redox potentials in both aqueous (Fig. 9, Table S5†) and acetonitrile solutions (Fig. S20, Table S4†). The Mo peaks have more positive potentials than the W peaks.[89] $PVMo_{11}$@HKUST and PVW_{11}@HKUST cyclic voltammograms (CVs) were collected by immobilizing the materials on glassy carbon working electrodes (Fig. 9). The observed V peaks in both POM@MOFs have potentials close to those of their homogeneous vanadium-containing POM counterparts.[43,59,73] Thermodynamically, Mo centers are much easier to reduce than W centers in the same POM structure, thus the former centers are more likely to engage in redox processes than the latter. This agrees with the fact that $PVMo$ can transfer multiple electrons including both V and Mo centers; whereas, PVW under identical experimental conditions, can only transfer one electron to a V center. Fig. S22† shows the CVs of $PCoW_{11}$ and $PNiW_{11}$ in pH = 5 acetate buffer. Both POMs have two redox peaks at negative potential (vs. RHE). Some transition-metal redox peaks overlap with W redox peaks consistent with a weaker oxidative ability than PVW_{11}.[90]

Conclusions

In this work, we give compelling evidence of synergistic electron transfer between POM and MOF framework in host–guest $PVMo$@HKUST materials. The kinetic and thermodynamic results indicate that PXW_{11} materials have limited electron transfer ability with Cu, thus when all the Cu(II) is reduced to Cu(I) via eqn (2) (Fig. 7), no Cu(II) sites remain in the MOF. As a result, the catalytic aerobic thiol removal reaction (deodorization) has limited conversion. The Cu(I) sites in the MOF nodes cannot be reoxidized back to Cu(II) via eqn (3), leading to distortion of the MOF framework. Therefore, POM@MOF synergism regarding activity parallels this synergism for POM@MOF stability.

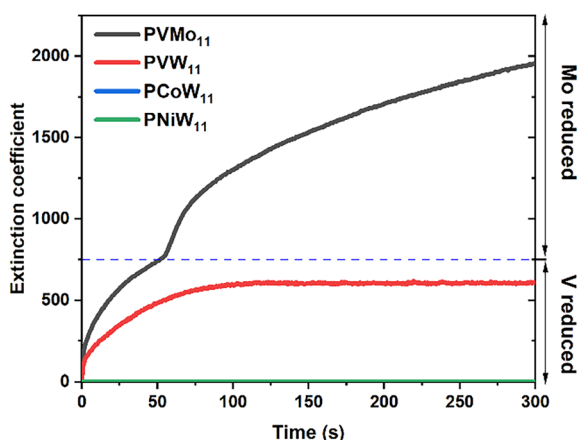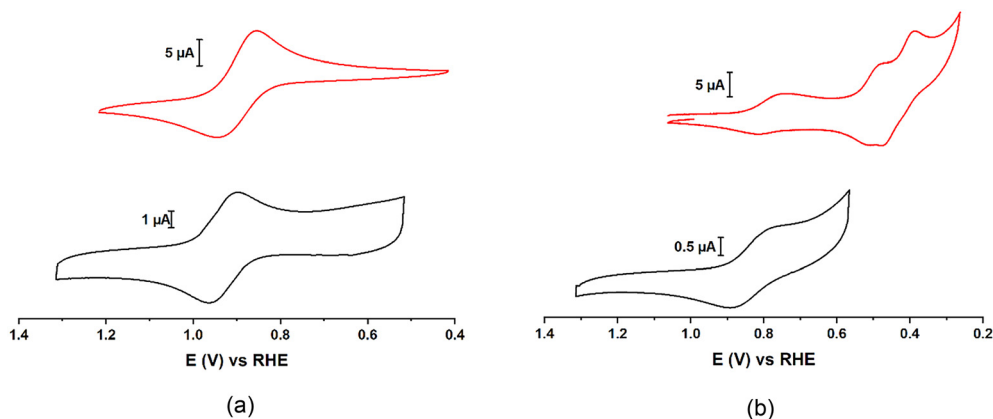**Fig. 8** Kinetics of 0.5 mM $PVMo_{11}$ and PVW_{11} reduction by 25 mM RSH under Ar catalyzed by 2 μM Cu(II) in pH = 2 H_2SO_4/Na_2SO_4 buffer, and 0.5 mM $PCoW_{11}$ and $PNiW_{11}$ reduction by 25 mM RSH under Ar catalyzed by 10 μM Cu(II) in pH = 5 sodium acetate buffer.

5100 | *Catal. Sci. Technol.*, 2023, **13**, 5094–5103

This journal is © The Royal Society of Chemistry 2023

Fig. 9 a) Black: cyclic voltammograms (CV) of homogeneous 0.5 mM $H_3PVW_{11}O_{40}$ (**PVW$_{11}$**) on glassy carbon (GC) electrode. Red: CV of **PVW$_{11}$**@HKUST immobilized on GC electrode. b) Black: CV of homogeneous 0.5 mM $H_3PVMo_{11}O_{40}$ (**PVMo$_{11}$**) on GC electrode. Red: CV of **PVMo$_{11}$**@HKUST immobilized on GC electrode. Conditions: pH = 2 H_2SO_4/Na_2SO_4 buffer, 0.1 M KNO_3, scan rate, v = 100 mV s^{-1}, T = 298 K. The immobilization can be proved by the linear relationship of I vs. v in Fig. S22.†

Author contributions

Xinlin Lu performed most of the experiments and drafted most of the article. Ting Cheng performed some of the electroanalytical experiments. Yurii V. Geletii oversaw the kinetics experiments and provided advice on the entire manuscript. John Bacsa performed the X-ray crystallography. Craig L. Hill oversaw all aspects of this study and did final editing of all documents.

Conflicts of interest

There are no conflicts of interest to declare.

Acknowledgements

References

1 J. X. Liu, X. B. Zhang, Y. L. Li, S. L. Huang and G. Y. Yang, *Coord. Chem. Rev.*, 2020, **414**, 213260.

2 D. Y. Du, J. S. Qin, S. L. Li, Z. M. Su and Y. Q. Lan, *Chem. Soc. Rev.*, 2014, **43**, 4615–4632.

3 J. Sun, S. Abednatanzi, P. Van Der Voort, Y. Y. Liu and K. Leus, *Catalysts*, 2020, **10**, 578.

4 M. Samaniyan, M. Mirzaei, R. Khajavian, H. Eshtiagh-Hosseini and C. Streb, *ACS Catal.*, 2019, **9**, 10174–10191.

5 M. Genovese and K. Lian, *Curr. Opin. Solid State Mater. Sci.*, 2015, **19**, 126–137.

6 Y. Liu, C. Tang, M. Cheng, M. Chen, S. Chen, L. Lei, Y. Chen, H. Yi, Y. Fu and L. Li, *ACS Catal.*, 2021, **11**, 13374–13396.

7 M. T. Pope and A. Müller, *Angew. Chem., Int. Ed. Engl.*, 1991, **30**, 34–48.

8 C. L. Hill and C. M. Prosser-McCartha, *Coord. Chem. Rev.*, 1995, **143**, 407–455.

9 C. L. Hill, L. Delannoy, D. C. Duncan, I. A. Weinstock, R. F. Renneke, R. S. Reiner, R. H. Atalla, J. W. Han, D. A. Hillesheim, R. Cao, T. M. Anderson, N. M. Okun, D. G. Musaev and Y. V. Geletii, *C. R. Chim.*, 2007, **10**, 305–312.

10 S. S. Wang and G. Y. Yang, *Chem. Rev.*, 2015, **115**, 4893–4962.

11 I. V. Kozhevnikov, *Chem. Rev.*, 1998, **98**, 171–198.

12 I. V. Kozhevnikov, *J. Mol. Catal. A: Chem.*, 1997, **117**, 151–158.

13 R. Neumann, *Inorg. Chem.*, 2010, **49**, 3594–3601.

14 I. A. Weinstock, R. E. Schreiber and R. Neumann, *Chem. Rev.*, 2018, **118**, 2680–2717.

15 N. Mizuno and M. Misono, *Chem. Rev.*, 1998, **98**, 199–218.

16 K. P. Sullivan, M. Wieliczko, M. Kim, Q. Yin, D. L. Collins-Wildman, A. K. Mehta, J. Bacsa, X. Lu, Y. V. Geletii and C. L. Hill, *ACS Catal.*, 2018, **8**, 11952–11959.

17 J. J. Walsh, A. M. Bond, R. J. Forster and T. E. Keyes, *Coord. Chem. Rev.*, 2016, **306**, 217–234.

18 T. Yamase, *Chem. Rev.*, 1998, **98**, 307–325.

19 E. Papaconstantinou, *Chem. Soc. Rev.*, 1989, **18**, 1–31.

20 C. Streb, *Dalton Trans.*, 2012, **41**, 1651–1659.

21 J. M. Cameron, D. J. Wales and G. N. Newton, *Dalton Trans.*, 2018, **47**, 5120–5136.

22 M. Tao, Q. Yin, A. L. Kaledin, N. Uhlikova, X. Lu, T. Cheng, Y. S. Chen, T. Lian, Y. V. Geletii, D. G. Musaev, J. Bacsa and C. L. Hill, *Inorg. Chem.*, 2022, **61**, 6252–6262.

23 I. A. Weinstock, *Chem. Rev.*, 1998, **98**, 113–170.

24 M. Sadakane and E. Steckhan, *Chem. Rev.*, 1998, **98**, 219–237.

25 N. Mizuno and M. Misono, *Chem. Rev.*, 1998, **98**, 199–217.

26 V. G. Snider and C. L. Hill, *J. Hazard. Mater.*, 2023, **442**, 130015.

27 H. Ma, B. Liu, B. Li, L. Zhang, Y. G. Li, H. Q. Tan, H. Y. Zang and G. Zhu, *J. Am. Chem. Soc.*, 2016, **138**, 5897–5903.

28 L. Vilà-Nadal and L. Cronin, *Nat. Rev. Mater.*, 2017, **2**, 1–15.

29 Q. Wang and D. Astruc, *Chem. Rev.*, 2020, **120**, 1438–1511.

30 Q. L. Zhu and Q. Xu, *Chem. Soc. Rev.*, 2014, **43**, 5468–5512.

31 J. L. C. Rowsell and O. M. Yaghi, *Microporous Mesoporous Mater.*, 2004, **73**, 3–14.

This journal is © The Royal Society of Chemistry 2023

Catal. Sci. Technol., 2023, **13**, 5094–5103 | **5101**

32 H. Furukawa, K. E. Cordova, M. O'Keeffe and O. M. Yaghi, *Science*, 2013, **341**, 1230444.

33 N. V. Maksimchuk, O. A. Kholdeeva, K. A. Kovalenko and V. P. Fedin, *Isr. J. Chem.*, 2011, **51**, 281–289.

34 J. Juan-Alcañiz, E. V. Ramos-Fernandez, U. Lafont, J. Gascon and F. Kapteijn, *J. Catal.*, 2010, **269**, 229–241.

35 G. Férey, C. Mellot-Draznieks, C. Serre, F. Millange, J. Dutour, S. Surblé and I. Margiolaki, *Science*, 2005, **309**, 2040–2042.

36 J. Song, Z. Luo, D. K. Britt, H. Furukawa, O. M. Yaghi, K. I. Hardcastle and C. L. Hill, *J. Am. Chem. Soc.*, 2011, **133**, 16839–16846.

37 C. Y. Sun, S. X. Liu, D. D. Liang, K. Z. Shao, Y. H. Ren and Z. M. Su, *J. Am. Chem. Soc.*, 2009, **131**, 1883–1888.

38 L. Yang, H. Naruke and T. Yamase, *Inorg. Chem. Commun.*, 2003, **6**, 1020–1024.

39 S. Ahn, S. L. Nauert, C. T. Buru, M. Rimoldi, H. Choi, N. M. Schweitzer, J. T. Hupp, O. K. Farha and J. M. Notestein, *J. Am. Chem. Soc.*, 2018, **140**, 8535–8543.

40 C. T. Buru, A. E. Platero-Prats, D. G. Chica, M. G. Kanatzidis, K. W. Chapman and O. K. Farha, *J. Mater. Chem. A*, 2018, **6**, 7389–7394.

41 C. T. Buru, P. Li, B. L. Mehdi, A. Dohnalkova, A. E. Platero-Prats, N. D. Browning, K. W. Chapman, J. T. Hupp and O. K. Farha, *Chem. Mater.*, 2017, **29**, 5174–5181.

42 C. T. Buru, M. C. Wasson and O. K. Farha, *ACS Appl. Nano Mater.*, 2020, **3**, 658–664.

43 W. Salomon, C. Roch-Marchal, P. Mialane, P. Rouschmeyer, C. Serre, M. Haouas, F. Taulelle, S. Yang, L. Ruhlmann and A. Dolbecq, *Chem. Commun.*, 2015, **51**, 2972–2975.

44 W. Xie and F. Wan, *Chem. Eng. J.*, 2019, **365**, 40–50.

45 Y. L. Peng, J. Liu, H. F. Zhang, D. Luo and D. Li, *Inorg. Chem. Front.*, 2018, **5**, 1563–1569.

46 L. Zeng, L. Xiao, Y. Long and X. Shi, *J. Colloid Interface Sci.*, 2018, **516**, 274–283.

47 R. Li, X. Ren, J. Zhao, X. Feng, X. Jiang, X. Fan, Z. Lin, X. Li, C. Hu and B. Wang, *J. Mater. Chem. A*, 2014, **2**, 2168–2173.

48 Q. Y. Li, L. Zhang, Y. X. Xu, Q. Li, H. Xue and H. Pang, *ACS Sustainable Chem. Eng.*, 2019, **7**, 5027–5033.

49 S. Mukhopadhyay, J. Debgupta, C. Singh, A. Kar and S. K. Das, *Angew. Chem., Int. Ed.*, 2018, **57**, 1918–1923.

50 G. Paille, M. Gomez-Mingot, C. Roch-Marchal, B. Lassalle-Kaiser, P. Mialane, M. Fontecave, C. Mellot-Draznieks and A. Dolbecq, *J. Am. Chem. Soc.*, 2018, **140**, 3613–3618.

51 X. Lu, T. Cheng, Y. V. Geletii and C. L. Hill, *Inorg. Chem.*, 2023, **5**, 2404–2414.

52 X. Lu, Y. V. Geletii, T. Cheng and C. L. Hill, Role of Multiple Vanadium Centers on Redox Buffering and Rates of Polyvanadomolybdate-Cu(II)-Catalyzed Aerobic Oxidations, *Inorg. Chem.*, 2023, **62**, 5822–5830.

53 Y. Liu, S. Liu, S. Liu, D. Liang, S. Li, Q. Tang, X. Wang, J. Miao, Z. Shi and Z. Zheng, *ChemCatChem*, 2013, **5**, 3086–3091.

54 X. Zhong, Y. Lu, F. Luo, Y. Liu, X. Li and S. Liu, *Chem. – Eur. J.*, 2018, **24**, 3045–3051.

55 J. Zhu, P. C. Wang and M. Lu, *Catal. Sci. Technol.*, 2015, **5**, 3383–3393.

56 J. Zhu, M. N. Shen, X. J. Zhao, P. C. Wang and M. Lu, *ChemPlusChem*, 2014, **79**, 872–878.

57 X. Xu, S. Chen, Y. Chen, H. Sun, L. Song, W. He and X. Wang, *Small*, 2016, **12**, 2982–2990.

58 H. Yang, J. Li, L. Wang, W. Dai, Y. Lv and S. Gao, *Catal. Commun.*, 2013, **35**, 101–104.

59 E. Rafiee and N. Nobakht, *J. Mol. Catal. A: Chem.*, 2015, **398**, 17–25.

60 Y. Liu, S. Liu, D. He, N. Li, Y. Ji, Z. Zheng, F. Luo, S. Liu, Z. Shi and C. Hu, *J. Am. Chem. Soc.*, 2015, **137**, 12697–12703.

61 L. H. Wee, S. R. Bajpe, N. Janssens, I. Hermans, K. Houthoofd, C. E. A. Kirschhock and J. A. Martens, *Chem. Commun.*, 2010, **46**, 8186–8188.

62 Z. Wang and Q. Chen, *Green Chem.*, 2016, **18**, 5884–5889.

63 L. H. Wee, C. Wiktor, S. Turner, W. Vanderlinden, N. Janssens, S. R. Bajpe, K. Houthoofd, G. Van Tendeloo, S. De Feyter, C. E. A. Kirschhock and J. A. Martens, *J. Am. Chem. Soc.*, 2012, **134**, 10911–10919.

64 D. Mustafa, E. Breynaert, S. R. Bajpe, J. A. Martens and C. E. A. Kirschhock, *Chem. Commun.*, 2011, **47**, 8037–8039.

65 C. R. Wade and M. Dincă, *Dalton Trans.*, 2012, **41**, 7931–7938.

66 S. R. Bajpe, C. E. A. Kirschhock, A. Aerts, E. Breynaert, G. Absillis, T. N. Parac-Vogt, L. Giebeler and J. A. Martens, *Chem. – Eur. J.*, 2010, **16**, 3926–3932.

67 E. A. Nagul, I. D. McKelvie, P. Worsfold and S. D. Kolev, *Anal. Chim. Acta*, 2015, **890**, 60–82.

68 N. Maksimchuk, M. Timofeeva, M. Melgunov, A. Shmakov, Y. Chesalov, D. Dybtsev, V. Fedin and O. Kholdeeva, *J. Catal.*, 2008, **257**, 315–323.

69 N. V. Maksimchuk, K. A. Kovalenko, S. S. Arzumanov, Y. A. Chesalov, M. S. Melgunov, A. G. Stepanov, V. P. Fedin and O. A. Kholdeeva, *Inorg. Chem.*, 2010, **49**, 2920–2930.

70 N. V. N. Maksimchuk, M. N. Timofeeva, M. S. Melgunov, A. N. A. Shmakov, Y. A. Chesalov, D. N. D. Dybtsev, V. P. Fedin and O. A. Kholdeeva, *J. Catal.*, 2008, **257**, 315–323.

71 N. V. N. Maksimchuk, M. N. Timofeeva, M. S. Melgunov, A. N. A. Shmakov, Y. A. Chesalov, D. N. D. Dybtsev, V. P. Fedin and O. A. Kholdeeva, *J. Catal.*, 2008, **257**, 315–323.

72 L. Bromberg, Y. Diao, H. Wu, S. A. Speakman and T. A. Hatton, *Chem. Mater.*, 2012, **24**, 1664–1675.

73 D. M. Fernandes, A. D. S. Barbosa, J. Pires, S. S. Balula, L. Cunha-Silva and C. Freire, *ACS Appl. Mater. Interfaces*, 2013, **5**, 13382–13390.

74 M. Yin, C. K. Wu, Y. Lou, C. Burda, J. T. Koberstein, Y. Zhu and S. O'Brien, *J. Am. Chem. Soc.*, 2005, **127**, 9506–9511.

75 C. Chen, T. Wu, D. Yang, P. Zhang, H. Liu, Y. Yang, G. Yang and B. Han, *Chem. Commun.*, 2018, **54**, 5984–5987.

76 T. Wei, M. Zhang, P. Wu, Y. J. Tang, S. L. Li, F. C. Shen, X. L. Wang, X. P. Zhou and Y. Q. Lan, *Nano Energy*, 2017, **34**, 205–214.

77 P. Zhu, X. Yang, X. Li, N. Sheng, H. Zhang, G. Zhang and J. Sha, *Dalton Trans.*, 2019, **49**, 79–88.

78 H. Liu, L. G. Gong, C. X. Wang, C. M. Wang, K. Yu and B. Bin Zhou, *J. Mater. Chem. A*, 2021, **9**, 13161–13169.

5102 | *Catal. Sci. Technol.*, 2023, **13**, 5094–5103

This journal is © The Royal Society of Chemistry 2023

79 P. St. Petkov, G. N. Vayssilov, J. Liu, O. Shekhah, Y. Wang, C. Wöll and T. Heine, *ChemPhysChem*, 2012, **13**, 2025–2029.

80 C. Chen, T. Wu, D. Yang, P. Zhang, H. Liu, Y. Yang, G. Yang and B. Han, *Chem. Commun.*, 2018, **54**, 5984–5987.

81 A. D. Leu and D. A. Armstrong, *J. Phys. Chem.*, 1986, **90**, 1449–1454.

82 V. Vortisch, P. Kroneck and P. Hemmerich, *J. Am. Chem. Soc.*, 1976, **98**, 2821–2826.

83 R. Trammell, K. Rajabimoghadam and I. Garcia-Bosch, *Chem. Rev.*, 2019, **119**, 2954–3031.

84 G. A. Bagiyan, I. K. Koroleva, N. V. Soroka and A. V. Ufimtsev, *Russ. Chem. Bull.*, 2003, **52**, 1135–1141.

85 G. Scrivens, B. C. Gilbert and T. C. P. Lee, *J. Chem. Soc., Perkin Trans. 2*, 1995, **9**, 955–963.

86 M. G. Gantman, I. G. Tarkhanova and Y. G. Kolyagin, *J. Sulfur Chem.*, 2016, **37**, 501–514.

87 P. W. Albro, J. T. Corbett and J. L. Schroeder, *J. Inorg. Biochem.*, 1986, **27**, 191–203.

88 G. A. Bagiyan, I. K. Koroleva, N. V. Soroka and A. V. Ufimtsev, *Kinet. Catal.*, 2004, **45**, 372–380.

89 J. J. Altenau, M. T. Pope, R. A. Prados and H. So, *Inorg. Chem.*, 1975, **14**, 417–421.

90 J. H. Choi, J. K. Kim, D. R. Park, T. H. Kang, J. H. Song and I. K. Song, *J. Mol. Catal. A: Chem.*, 2013, **371**, 111–117.

This journal is © The Royal Society of Chemistry 2023

Catal. Sci. Technol., 2023, **13**, 5094–5103 | **5103**